

Z' induced forward dominant processes in μ TRISTAN experiment

Arindam Das^{1,2,*} and Yuta Orikasa^{3,†}

¹*Institute for the Advancement of Higher Education, Hokkaido University, Sapporo 060-0817, Japan*

²*Department of Physics, Hokkaido University, Sapporo 060-0810, Japan*

³*Institute of Experimental and Applied Physics, Czech Technical University in Prague, Husova 240/5, 110 00 Prague 1, Czech Republic*

General $U(1)$ extension of the Standard Model (SM) is a well motivated beyond the Standard Model(BSM) scenario where three generations of right handed neutrinos (RHNs) are introduced to cancel gauge and mixed gauge-gravity anomalies. After the $U(1)_X$ is broken, RHNs participate in the seesaw mechanism to generate light neutrino masses satisfying neutrino oscillation data. In addition to that, a neutral gauge boson Z' is evolved which interacts with the left and right handed fermions differently manifesting chiral nature of the model which could be probed in future collider experiments. As a result, if we consider μ^+e^- and $\mu^+\mu^+$ collisions in μ TRISTAN experiment Z' mediated $2 \rightarrow 2$ scattering will appear in t - and u -channels depending on the initial and final states being accompanied by the photon and Z mediated interactions. This will result well motivated resulting forward dominant scenarios giving rise to sizable left-right asymmetry. Estimating constraints on general $U(1)$ coupling from LEP-II and LHC for different $U(1)_X$ charges, we calculate differential and integrated scattering cross section and left-right asymmetry for $\mu^+e^- \rightarrow \mu^+e^-$ and $\mu^+\mu^+ \rightarrow \mu^+\mu^+$ processes which could be probed at μ TRISTAN experiment further enlightening the interaction between Z' and charged leptons and the $U(1)_X$ breaking scale.

I. INTRODUCTION

Standard Model (SM) can not explain the observation of tiny neutrino mass and flavor mixing, dark matter relic density and matter-antimatter asymmetry in the universe [1] which allow us to propose theories beyond the SM (BSM). An interesting but simple extension of the SM which caters these aspects could be realized in the form $U(1)$ extension where three generations of right-handed neutrinos (RHNs) could be involved to explain the origin of tiny neutrino mass through seesaw mechanism along with an SM-singlet scalar field, responsible for the neutrino mass generation mechanism. Such scenarios are associated with an additional neutral gauge boson, commonly known as Z' which has very rich phenomenological aspects [2, 3]. There are many ultraviolet-complete scenarios where Z' boson arises naturally, for example, Left-Right symmetric models [4–6], grand unification [7, 8] based on $SO(10)$ and E_6 [9, 10] theories, respectively. There is another interesting example of where $U(1)$ extension of the SM comes up with neutrino mass and aspects of dark matter and matter-antimatter asymmetry is commonly known as $B-L$ (baryon minus lepton) scenario [11–14] where Z' arises naturally and acquires mass after the $B-L$ symmetry breaking. Z' induced scenarios are under scanner for a long period of time starting from LEP [15] and Tevatron [16, 17], however, stringent bounds on the Z' mass and $U(1)$ gauge coupling comes from dilepton searches [18, 19] at the LHC superseding low-energy electroweak constraints [20].

In this paper we investigate a general $U(1)_X$ extension of the SM which includes three generations of SM-singlet RHNs and an SM-singlet scalar which helps to break the general $U(1)_X$ symmetry by which seesaw scenario is induced to generate tiny neutrino mass followed by the generation of mass of the BSM neutral gauge boson Z' . In our analysis we consider the situation where $U(1)_X$ charge assignment for the fermions do not depend on the generations. Reproducing the SM Yukawa interactions in the model structure we find that the $U(1)_X$ charge assignment of the SM charged fermions can be identified as the linear combination of charges of $U(1)_Y$ in SM and $U(1)_{B-L}$ gauge groups [21–25]. Hence the $U(1)_X$ scenario is a generalization of the $U(1)_{B-L}$ extension of the SM. Due to the gauge structure of the model we find that after solving the gauge and mixed gauge-gravity anomaly equations we find that Z' interacts differently with left and right handed fermions manifesting chiral nature of the model. In this paper we will focus on this property of the general $U(1)_X$ extension of the SM in the context of a muon-positron collider and multi-TeV same sign muon collider [26–35] at μ TRISTAN experiment where ultra-cold anti-muon technology can be used from J-PARC [36] experiment. In this experiment μ^+e^- collision could take place at the center of mass nergy $\sqrt{s} = 346$ GeV where the energy of the μ^+ beam is $E_\mu = 1$ TeV and that of the e^- beam is $E_e = 30$ GeV. Therefore center of mass energy of μ^+e^- collider can be derived as $\sqrt{s} = 2\sqrt{E_\mu E_e}$ and that could attain a luminosity of 1 ab^{-1} . This

* adas@particle.sci.hokudai.ac.jp

† yuta.orikasa@utef.cvut.cz

Gauge group	q_L^i	u_R^i	d_R^i	ℓ_L^i	e_R^i	N_R^i	H	Φ
$SU(3)_C$	3	3	3	1	1	1	1	1
$SU(2)_L$	2	1	1	2	1	1	2	1
$U(1)_Y$	1/6	2/3	-1/3	-1/2	-1	0	1/2	0
$U(1)_X$	$\tilde{x}_q = \frac{1}{6}x_H + \frac{1}{3}x_\Phi$	$\tilde{x}_u = \frac{2}{3}x_H + \frac{1}{3}x_\Phi$	$\tilde{x}_d = -\frac{1}{3}x_H + \frac{1}{3}x_\Phi$	$\tilde{x}_\ell = -\frac{1}{2}x_H - x_\Phi$	$\tilde{x}_e = -x_H - x_\Phi$	$\tilde{x}_\nu = -x_\Phi$	$-\frac{x_H}{2}$	$2x_\Phi$

Table I. Particle content of the minimal $U(1)_X$ model where $i(= 1, 2, 3)$ is generation index.

could be upgraded to a $\mu^+\mu^+$ collider where center of mass energy could reach at $\sqrt{s} = 2$ TeV or higher where muon beam energy could be at least 1 TeV. This collider could attain a luminosity of 100 fb^{-1} . Such machines could be potentially rich for a variety of phenomenological aspects involving physics beyond the SM apart from being a Higgs factory [37–44].

Due to the presence of the Z' boson under the general $U(1)_X$ extension, we study $\mu^+e^- \rightarrow \mu^+e^-$ process mediated by Z , γ and Z' in the t -channel. This is process is forward dominant and therefore at μ TRISTAN collider left-right asymmetry (\mathcal{A}_{LR}) will be an interesting variable to study the influence of Z' . On the other hand in the case of $\mu^+\mu^+$ collision we study \mathcal{A}_{LR} from the Z , γ and Z' mediated $\mu^+\mu^+ \rightarrow \mu^+\mu^+$ in t - and u -channels. We involve corresponding interference terms in our analysis depending on the nature of the collision. In both the cases we first estimate total scattering cross section and estimate its deviation from the SM processes mediated by Z and γ . In the case of $U(1)_X$ scenario, there will be additional Z' mediated processes and the corresponding interferences will affect these processes. Therefore we estimate the corresponding total scattering cross sections and their deviations from the SM. In the case of general $U(1)_X$ scenario we can vary the $U(1)_X$ charges to estimate the deviations in scattering cross section and \mathcal{A}_{LR} . The effect of $U(1)_X$ charges will appear through the Z' vertices with electron and muon. As a result chiral nature of the model could be investigated in μ TRISTAN experiment.

The paper is organized as follows. We discuss the general $U(1)_X$ model in Sec. II. We calculate total scattering cross sections for $\mu^+e^- \rightarrow \mu^+e^-$ and $\mu^+\mu^+ \rightarrow \mu^+\mu^+$ processes and we also estimate differential and integrated LR asymmetry in Sec. III. Finally we conclude the paper in Sec. IV.

II. $U(1)$ EXTENDED SCENARIOS AND Z' INTERACTIONS

We consider a general $U(1)_X$ extension of the SM following the gauge structure $SU(3)_C \otimes SU(2)_L \otimes U(1)_Y \otimes U(1)_X$ and the particle content is given in Tab. I. The model consists of three generations of the RHNs (N_R^i) and an SM-singlet BSM scalar (Φ) apart from the SM particles. The RHNs are induced to cancel gauge and mixed gauge-gravity anomalies following the corresponding anomaly conditions given below:

$$\begin{aligned}
U(1)_X \otimes [SU(3)_C]^2 & : & 2\tilde{x}_q - \tilde{x}_u - \tilde{x}_d & = 0 , \\
U(1)_X \otimes [SU(2)_L]^2 & : & 3\tilde{x}_q + \tilde{x}_\ell & = 0 , \\
U(1)_X \otimes [U(1)_Y]^2 & : & \tilde{x}_q - 8\tilde{x}_u - 2\tilde{x}_d + 3\tilde{x}_\ell - 6\tilde{x}_e & = 0 , \\
[U(1)_X]^2 \otimes U(1)_Y & : & \tilde{x}_q^2 - 2\tilde{x}_u^2 + \tilde{x}_d^2 - \tilde{x}_\ell^2 + \tilde{x}_e^2 & = 0 , \\
[U(1)_X]^3 & : & 6\tilde{x}_q^3 - 3\tilde{x}_u^3 - 3\tilde{x}_d^3 + 2\tilde{x}_\ell^3 - \tilde{x}_\nu^3 - \tilde{x}_e^3 & = 0 , \\
U(1)_X \otimes [\text{grav.}]^2 & : & 6\tilde{x}_q - 3\tilde{x}_u - 3\tilde{x}_d + 2\tilde{x}_\ell - \tilde{x}_\nu - \tilde{x}_e & = 0 , \tag{1}
\end{aligned}$$

respectively. We write down the Yukawa interactions in the model involving SM and BSM particles following the gauge structure $\mathcal{G}_{SM} \otimes U(1)_X$ as

$$\mathcal{L}^{\text{Yukawa}} = -Y_u^{\alpha\beta} \overline{q_L^\alpha} H u_R^\beta - Y_d^{\alpha\beta} \overline{q_L^\alpha} \tilde{H} d_R^\beta - Y_e^{\alpha\beta} \overline{\ell_L^\alpha} \tilde{H} e_R^\beta - Y_\nu^{\alpha\beta} \overline{\ell_L^\alpha} H N_R^\beta - Y_N^\alpha \Phi (\overline{N_R^\alpha})^c N_R^\alpha + \text{H.c.} , \tag{2}$$

where SM Higgs doublet field can be denoted by H following the transformation rule \tilde{H} following $i\tau^2 H^*$ where τ^2 is the second Pauli matrix. Now following charge neutrality in the context of Yukawa interactions given in Eq. (2) we write the following relations between the $U(1)_X$ charges of the particles as

$$\begin{aligned}
-\frac{1}{2}x_H & = -\tilde{x}_q + \tilde{x}_u = \tilde{x}_q - \tilde{x}_d = \tilde{x}_\ell - \tilde{x}_e = -\tilde{x}_\ell + \tilde{x}_\nu , \\
2x_\Phi & = -2\tilde{x}_\nu . \tag{3}
\end{aligned}$$

Solving Eqs. (1) and (3) we obtain the $U(1)_X$ charges of the particles in the model in terms of the charges of the scalar fields x_H and x_Φ . The charges are given in the Tab. I. We find that after anomaly cancellation, the charges are written as a linear combination of $U(1)_Y$ and $U(1)_{B-L}$ charges. Hence note that left and right handed fermions are differently charged under the $U(1)_X$ gauge group leading to chiral nature of the model while these particles interact with the neutral BSM gauge boson Z' . In our analysis we fix $x_\Phi = 1$ without the loss of generality and vary x_H showing interesting properties. If we fix $x_H = -2$, we find that left handed fermions do not interact with Z' , however, right handed fermions do. This is $U(1)_R$ scenario while for $x_H = 0$ we find that left and right handed fermions interact equally with Z' reproducing a vector-like scenario commonly known as B-L model. In addition to that we fix $x_H = -1$ when e_R does not interact with Z' , however, ℓ_L does. Similarly for $x_H = 1$, the $U(1)_X$ charge of d_R becomes zero disallowing its interaction with Z' . For simplicity we fix $x_H = 2$ where all left and right handed fermions interact with Z' , however, their $U(1)_X$ charges are different manifesting the chiral nature of the model. In our analysis we will study the left right asymmetry from the $\mu^+e^- \rightarrow \mu^+e^-$ and $\mu^+\mu^+ \rightarrow \mu^+\mu^+$ forward dominant processes, therefore we confine ourselves in the chiral scenarios only. The renormalizable scalar potential of this model can be written as

$$V = m_H^2(H^\dagger H) + \lambda_H(H^\dagger H)^2 + m_\Phi^2(\Phi^\dagger \Phi) + \lambda_\Phi(\Phi^\dagger \Phi)^2 + \lambda_{\text{mix}}(H^\dagger H)(\Phi^\dagger \Phi) , \quad (4)$$

where H and Φ can be separately approximated in the analysis of scalar potential considering λ_{mix} to be very small. After the $U(1)_X$ symmetry breaking and the electroweak symmetry breaking, the scalar fields develop vacuum expectation values (VEVs) as

$$\langle H \rangle = \frac{1}{\sqrt{2}} \begin{pmatrix} v+h \\ 0 \end{pmatrix} \quad \text{and} \quad \langle \Phi \rangle = \frac{v_\Phi + \phi}{\sqrt{2}} , \quad (5)$$

where $v = 246$ GeV is the electroweak scale VEV at the potential minimum and v_Φ is a free parameter. After the breaking of $U(1)_X$ symmetry, the neutral BSM gauge boson Z' acquires the following mass term as

$$M_{Z'} = 2g_X v_\Phi , \quad (6)$$

considering $v_\Phi \gg v$ and $x_\Phi = 1$ and here g_X is general $U(1)_X$ coupling. Here Z' mass is a free parameter.

From the Yukawa interactions given in Eq. (2), we find that the RHNs interact with the SM-singlet scalar field Φ generates Majorana mass term for heavy neutrinos after the breaking of the general $U(1)$ symmetry. After the electroweak symmetry breaking, the Dirac mass term is generated from the interaction among the SM-singlet RHN, SM like Higgs doublet and SM lepton doublet switching on the seesaw mechanism from

$$m_{N_R^\alpha} = \frac{Y_N^\alpha v_\Phi}{\sqrt{2}}, \quad m_D^{\alpha\beta} = \frac{Y_\nu^{\alpha\beta} v}{\sqrt{2}} \quad (7)$$

which are Majorana and Dirac mass terms respectively to originate the tiny neutrino masses and flavor mixing. Hence neutrino mass matrix can be written as

$$m_\nu = \begin{pmatrix} 0 & m_D \\ m_D^T & m_N \end{pmatrix}. \quad (8)$$

Finally diagonalizing Eq. 8 we obtain the light neutrino mass eigenvalues as $-m_D m_N^{-1} m_D^T$. As neutrino mass generation is not the main motivation of this paper therefore we skip giving much details of it.

The interaction between the Z' gauge boson and SM charged fermions can be written as

$$\mathcal{L}_{\text{int}} = -g_X (\bar{q}\gamma^\mu \tilde{x}_q P_L q + \bar{u}\gamma^\mu \tilde{x}_u P_R u + \bar{d}\gamma^\mu \tilde{x}_d P_R d) Z'_\mu - g_X (\bar{\ell}\gamma^\mu \tilde{x}_\ell P_L \ell + \bar{e}\gamma^\mu \tilde{x}_e P_R e) Z'_\mu, \quad (9)$$

where $\tilde{x}_u, \tilde{x}_d, \tilde{x}_\ell$ and \tilde{x}_e are the corresponding charges which could be obtained from Tab. I. In our paper Z' interaction with charged leptons are the relevant ones. Here P_L and P_R are the left and right projection operators $(1 \mp \gamma_5)/2$ respectively. Now we show the partial decay widths of Z' into different modes using Eq. (9). The partial decay widths of Z' into the SM charged fermions can be written as

$$\Gamma(Z' \rightarrow f\bar{f}) = N_c \frac{M_{Z'}}{24\pi} \left(g_L^f [g_X, x_H, x_\Phi]^2 + g_R^f [g_X, x_H, x_\Phi]^2 \right), \quad (10)$$

where $N_c = 3$ (1) is a color factor for the quarks (leptons) and $g_{L(R)}^f [g_X, x_H, x_\Phi]$ is the coupling of the Z' with the left (right) handed charged fermions from SM and these couplings depend on the $U(1)_X$ charges. The partial decay width of the Z' into light neutrinos can be written as

$$\Gamma(Z' \rightarrow \nu\bar{\nu}) = 3 \frac{M_{Z'}}{24\pi} g_L^\nu [g_X, x_H, x_\Phi]^2. \quad (11)$$

Machine	\sqrt{s}	95% CL lower limit on $M_{Z'}/g_X$ (in TeV)				
		$x_H = -2$	$x_H = -1$	$x_H = 0$	$x_H = 1$	$x_H = 2$
LEP-II	209 GeV	5.0	2.2	7.0	11.1	18.0
ILC	250 GeV	31.6	16.3	48.2	79.0	113.7
	500 GeV	54.4	26.3	81.6	139.1	199.7
	1 TeV	88.6	47.7	137.2	238.2	339.2

Table II. The 95% CL lower limits on $M_{Z'}/g_X$ in the $U(1)_X$ model from $e^+e^- \rightarrow f\bar{f}$ processes for different x_H and taking the most stringent limit out of all the different channels considered there.

The partial decay width of the Z' into a pair of RHNs for three generations can be written as

$$\Gamma(Z' \rightarrow NN) = 3 \frac{M_{Z'}}{24\pi} g_R^N [g_X, x_\Phi]^2 \left(1 - 4 \frac{m_N^2}{M_{Z'}^2}\right)^{\frac{3}{2}}. \quad (12)$$

However, in this analysis we assume for simplicity that the decay of the Z' into a pair of RHNs is kinematically disallowed because $m_N > M_{Z'}$.

Now we calculate bounds on g_X with respect to $M_{Z'}$. We calculate the limits on model parameters from the LEP experiment first for different x_H taking $M_{Z'} \gg \sqrt{s}$ in consideration. Following [15, 45, 46] and utilizing contact interaction for the process $e^-e^+ \rightarrow f\bar{f}$ we finally parametrize

$$\mathcal{L}_{\text{eff}} = \frac{g_X^2}{(1 + \delta_{ef})(\Lambda_{AB}^{f\pm})^2} \sum_{A,B=L,R} \eta_{AB} (\bar{e}\gamma^\mu P_A e) (\bar{f}\gamma_\mu P_B f), \quad (13)$$

where $g_X^2/4\pi$ is taken to be 1 by convention where $\delta_{ef} = 1$ (0) for $f = e$ ($f \neq e$), $\eta_{AB} = \pm 1$ or 0, and $\Lambda_{AB}^{f\pm}$ is considered as the scale of contact interaction. Here we consider constructive (+) or destructive (-) interference with SM processes $e^+e^- \rightarrow f\bar{f}$ [47]. Following [48] we evaluate Z' exchange matrix element in $U(1)_X$ case as

$$\frac{g'^2}{M_{Z'}^2 - s} [\bar{e}\gamma^\mu (\tilde{x}_\ell P_L + \tilde{x}_e P_R) e] [\bar{f}\gamma_\mu (\tilde{x}_{f_L} P_L + \tilde{x}_{f_R} P_R) f], \quad (14)$$

where \tilde{x}_{f_L} and \tilde{x}_{f_R} are $U(1)_X$ charges of f_L and f_R respectively which can be found in Table I. Now we match Eqs. (13) and (14) to obtain

$$M_{Z'}^2 \gtrsim \frac{g'^2}{4\pi} |x_{e_A} x_{f_B}| (\Lambda_{AB}^{f\pm})^2, \quad (15)$$

considering $M_{Z'}^2 \gg s$ where $\sqrt{s} = 209$ GeV for LEP-II. Hence we estimate bounds on $M_{Z'}/g_X$ from LEP using different values of $\Lambda_{AB}^{f\pm}$ for different values of x_H . To do that we use 95% bounds on $\Lambda_{AB}^{f\pm}$ from [15] for leptons and quarks taking $AB = LL, RR, LR, RL, VV$ and AA assuming universality in the contact interactions. In the same way we estimate prospective limits on $M_{Z'}/g_X$ for different x_H at ILC with $\sqrt{s} = 250$ GeV, 500 GeV and 1 TeV using the bounds on $\Lambda_{AB}^{f\pm}$ from [49]. We show these bounds in Fig. 1 where we find that LEP-II puts a stringent bound on $M_{Z'}/g_X$ and prospective limits from ILC could be stronger. The corresponding limits at 95% C. L. for different x_H are shown in Tab. II. Finally solving $M_{Z'}/g_X$ bounds for different x_H and for a range of $M_{Z'}$, we estimate limits on $g_X - M_{Z'}$ plane for different x_H and the limits are shown in Fig. 2 for LEP-II (green dotted) and prospective ILC (magenta dot-dashed, dashed and dotted), respectively. We calculate limits on $g_X - M_{Z'}$ for different x_H from the dilepton [18, 19] searches at the LHC using CMS and ATLAS results. We first estimate dilepton signal for electron and muon involving Z' from the model σ_{Model} considering a trial value of g_{Model} for a given x_H and different $M_{Z'}$ at $\sqrt{s} = 14$ TeV. Now we compare these cross sections with observed cross section from ATLAS and CMS ($\sigma_{\text{Obs.}}$) and using

$$g' = \sqrt{g_{\text{Model}}^2 \left(\frac{\sigma_{\text{Obs.}}}{\sigma_{\text{Model}}} \right)}. \quad (16)$$

Hence we calculate 95% limits on $g_X - M_{Z'}$ plane for different x_H . We also consider the future high-luminosity phase of the LHC (HL-LHC) at $\sqrt{s} = 14$ TeV with 3 ab^{-1} integrated luminosity and draw the projected dilepton bounds using

$$g_X^{\text{projected}} = g_X^{\text{current}} \sqrt{\frac{139(140) \text{fb}^{-1}}{\mathcal{L}_{\text{projected}}}}. \quad (17)$$

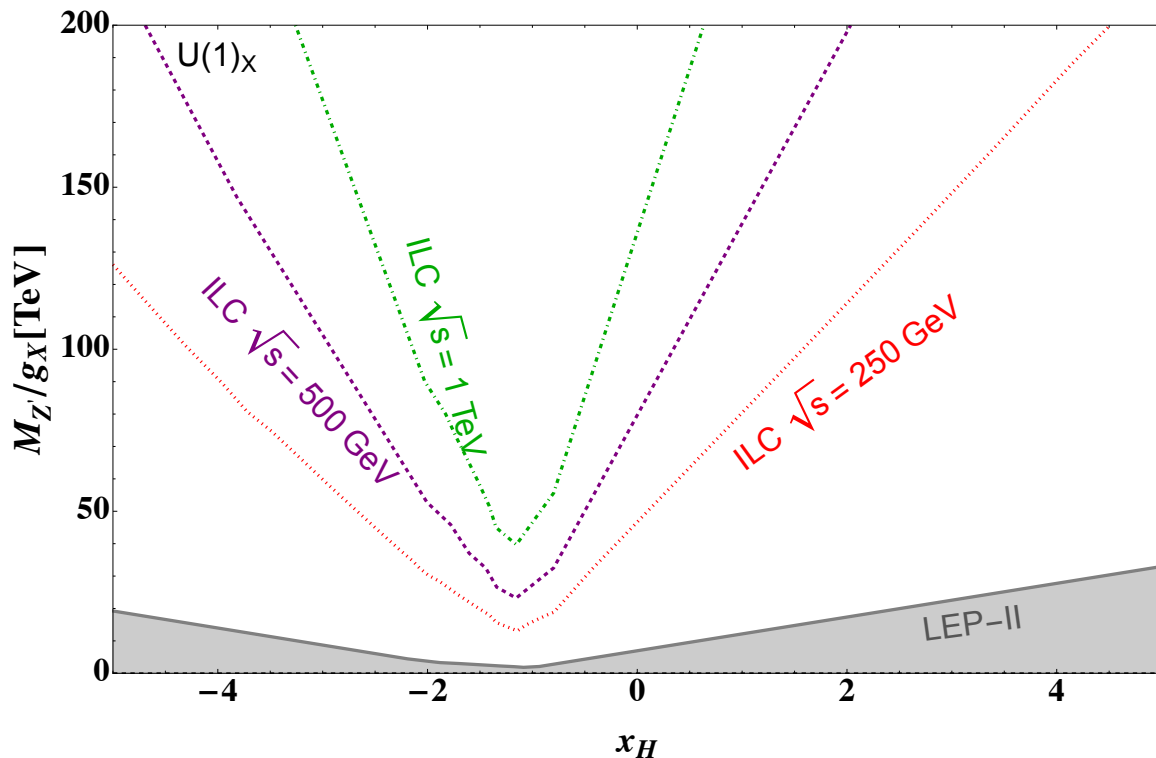


Figure 1. Limits on $M_{Z'}/g_X$ vs x_H in $U(1)_X$ scenario for LEP-II and prospective ILC in e^-e^+ collision. The LEP-II limits rule out the parameter space shown by gray shaded region. Prospective limits from ILC using e^-e^+ collisions are shown by different colored lines without shading.

The corresponding limits for CMS (blue dot-dashed) and ATLAS (red solid) for 2ℓ are shown in Fig. 2 for 139 fb^{-1} and 140 fb^{-1} luminosities. The scaled results for CMS (blue dashed) and ATLAS (red dashed) at 3 ab^{-1} are also shown in the same figure. The shaded regions are ruled out by existing experiments. For further analysis we consider $M_{Z'} = 7.5 \text{ TeV}$ and $g_X = 1$ for $x_H = -2, -1$ and 0 where as for same $M_{Z'}$ we consider $g_X = 0.6$ and 0.5 for $x_H = 1$ and $x_H = 2$ respectively.

III. SCATTERING CROSS SECTION AND LEFT-RIGHT ASYMMETRY

We consider the $2 \rightarrow 2$ scattering in the context of μ -TRISTAN experiment where we first consider the initial states as μ^+e^- and then $\mu^+\mu^+$ where we have forward dominant processes through t -channel and u -channel depending on the final states. Therefore in case μ -TRISTAN experiment to study the effect of Z' deviations in scattering cross sections from the SM and left-right asymmetry will be suitable observables to investigate in the following:

μ^+e^- collider

We consider the $\mu^+e^- \rightarrow \mu^+e^-$ scattering in the center-of-mass frame. Fig. 3 shows the $\mu^+e^- \rightarrow \mu^+e^-$ scattering processes. There are photon, Z and Z' mediated t -channel processes. We define the quantities p_1 as initial muon momentum, p_2 as initial electron momentum, k_1 as final muon momentum, k_2 as final electron momentum. The 4-vector representation of these momenta are $p_1 = (E_\mu, 0, 0, E_\mu)$, $p_2 = (E_e, 0, 0, -E_e)$, $k_1 = (E_1, 0, E_1 \sin \theta, E_1 \cos \theta)$ and $k_2 = (E_\mu + E_e - E_1, 0, -E_1 \sin \theta, E_\mu - E_e - E_1 \cos \theta)$, where E_μ is the initial muon energy, E_e is the initial electron energy, θ is the scattering angle of the muon and $E_1 = (2E_\mu E_e)/(E_\mu + E_e - (E_\mu - E_e) \cos \theta)$. The Mandelstam variables are given by

$$s_e = 4E_\mu E_e, \quad t_e = -2E_\mu E_1(1 - \cos \theta), \quad u_e = -2E_e E_1(1 + \cos \theta). \quad (18)$$

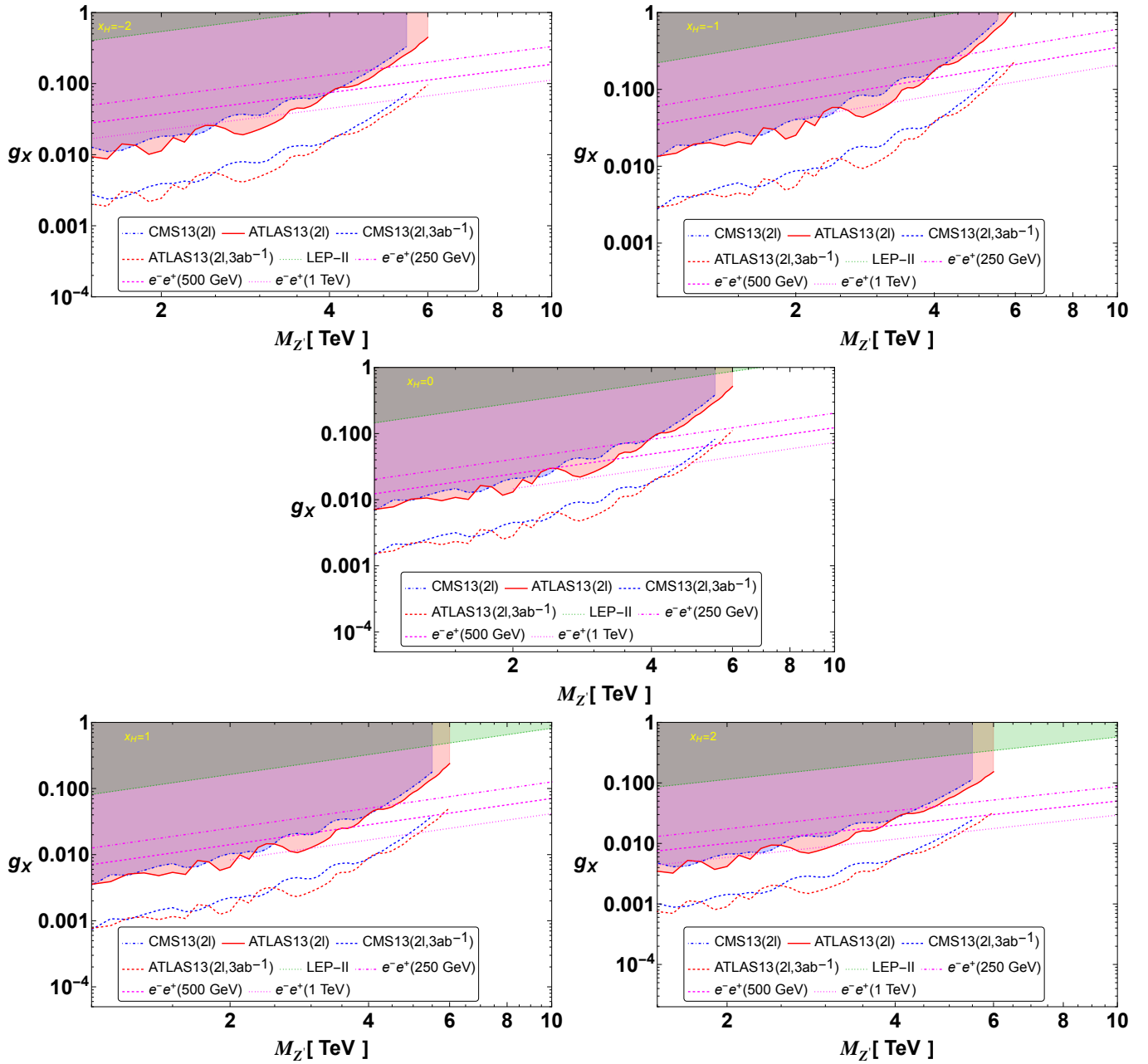


Figure 2. 95% upper limits on $g_X - M_{Z'}$ plane for different x_H . The shaded regions are ruled out by LEP-II (green), CMS (blue) and ATLAS (red) experiments respectively. The prospective limits are coming from e^-e^+ collisions in ILC at $\sqrt{s} = 250$ GeV, 500 GeV and 1 TeV by magenta dot-dashed, dashed and dotted lines respectively. Prospective limits from LHC (ATLAS and CMS) at 3 ab^{-1} luminosity shown by dashed blue and red lines.

We fix the energies, $E_\mu = 1 \text{ TeV}$, $E_e = 30 \text{ GeV}$ and the center-of-mass energy $\sqrt{s_e} = 346 \text{ GeV}$. We define the following quantities

$$\begin{aligned}
 T_{RR}^e &\equiv \sum_{V=\{\gamma, Z, Z'\}} \frac{g_L^{V\mu} g_R^{Ve}}{t_e - M_V^2}, & T_{LL}^e &\equiv \sum_{V=\{\gamma, Z, Z'\}} \frac{g_R^{V\mu} g_L^{Ve}}{t_e - M_V^2}, \\
 T_{RL}^e &\equiv \sum_{V=\{\gamma, Z, Z'\}} \frac{g_L^{V\mu} g_L^{Ve}}{t_e - M_V^2}, & T_{LR}^e &\equiv \sum_{V=\{\gamma, Z, Z'\}} \frac{g_R^{V\mu} g_R^{Ve}}{t_e - M_V^2}.
 \end{aligned} \tag{19}$$

where M_V and Γ_V are the mass and total decay width of the corresponding gauge bosons (except photon). We

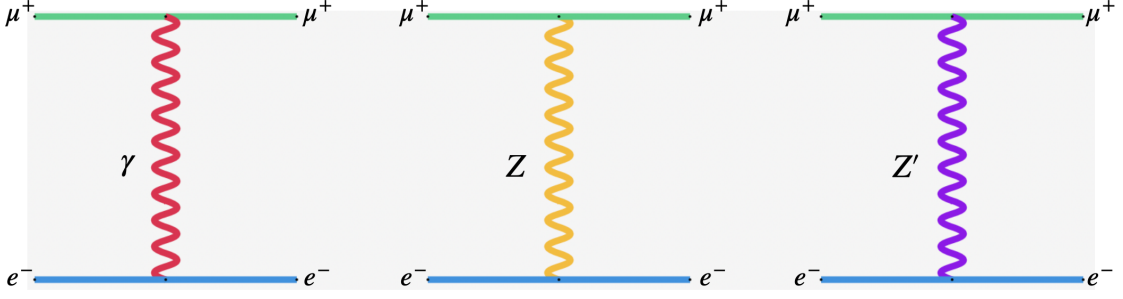


Figure 3. Photon, Z and Z' mediated $\mu^+e^- \rightarrow \mu^+e^-$ processes in t -channel at μ TRISTAN experiment with $\sqrt{s} = 346$ GeV where muon beam energy is 1 TeV and electron beam energy is 30 GeV.

present the quantities $|t_e T_{ij}^e|$ with $(i, j) = (L, R)$ in Fig. 4 for different x_H . The contributions from T_{RR}^e and T_{LL}^e coincide with each other because $g_L^{V_\mu} = g_L^{V_e}$ and $g_R^{V_e} = g_R^{V_\mu}$ because our model set-up is generation independent. On the other hand contributions from T_{RL}^e and T_{LR}^e are different because they depend on $g_L^{V_\mu} g_L^{V_e}$ and $g_R^{V_\mu} g_R^{V_e}$ respectively. However, these contributions depend on x_H . We find that left handed lepton doublets do not interact with Z' when $x_H = -2$ whereas right handed leptons do not interact with Z' when $x_H = -1$. In the case of $x_H = 0$, the left and right handed leptons interact equally. Due to this nature the pattern of contribution is different from other charges. In the case of $x_H = 1$ and 2, interactions of all left and right handed leptons with Z' are different manifesting chiral scenarios. Therefore the pattern of contributions from $x_H = 1$ and $x_H = 2$ are the same, however, different in magnitude. The quantities $|t_e T_{ij}^e|$ with $(i, j) = (L, R)$ involve effects from the t -channel process involving the individual contributions and corresponding interference of $\{\gamma, Z, Z'\}$ mediated interactions which grow with \sqrt{s} with $\cos \theta = 0.5$ and $M_{Z'} = 7.5$ TeV and after $\sqrt{s} = 10$ TeV, the contributions become flat.

Using the quantities given in Eq. 19, we can obtain the differential scattering cross sections with polarized initial states as the followings,

$$\frac{d\sigma_{\mu_R e_R}}{d\cos\theta} = \frac{u_e^2}{8\pi s_e} |T_{RR}^e|^2, \quad \frac{d\sigma_{\mu_L e_L}}{d\cos\theta} = \frac{u_e^2}{8\pi s_e} |T_{LL}^e|^2, \quad \frac{d\sigma_{\mu_R e_L}}{d\cos\theta} = \frac{s_e}{8\pi} |T_{RL}^e|^2, \quad \frac{d\sigma_{\mu_L e_R}}{d\cos\theta} = \frac{s_e}{8\pi} |T_{LR}^e|^2. \quad (20)$$

When initial muon and electron are longitudinally polarized, the differential scattering cross section is given by

$$\begin{aligned} \frac{d\sigma^e}{d\cos\theta}(P_\mu, P_e) = & \frac{1}{4} \left((1+P_\mu)(1+P_e) \frac{d\sigma_{\mu_R e_R}}{d\cos\theta} + (1-P_\mu)(1-P_e) \frac{d\sigma_{\mu_L e_L}}{d\cos\theta} \right. \\ & \left. + (1+P_\mu)(1-P_e) \frac{d\sigma_{\mu_R e_L}}{d\cos\theta} + (1-P_\mu)(1+P_e) \frac{d\sigma_{\mu_L e_R}}{d\cos\theta} \right), \end{aligned} \quad (21)$$

where P_μ and P_e are the polarization of the muon and electron beams. $P_i = +1$ denotes purely right-handed initial particles and $P_i = -1$ denotes purely left-handed initial particles. The deviation of the differential cross section of $U(1)_X$ case from the SM scenario is given by

$$\Delta_{d\sigma^e} \equiv \frac{\left[\frac{d\sigma^e}{d\cos\theta}(0,0) \right]_{U(1)_X}}{\left[\frac{d\sigma^e}{d\cos\theta}(0,0) \right]_{SM}} - 1. \quad (22)$$

Fig. 5 shows the deviation of the differential cross section from the SM showing the difference of the charges as a function of $\cos \theta$. We find that the deviation grows with $\cos \theta$ and reaches a saturation when $\cos \theta < 0.2$. We find that the deviation can be maximum for $x_H = 2$ reaching at 4% whereas that is minimum for $x_H = -1$ and the value is 0.2% where right handed leptons have no interaction with Z' . We also mention that the deviation reaches at 1.6% for $x_H = -2$, that for $x_H = 0$ is 2.2% and 2.75% for $x_H = 1$, respectively where $x_H = -2$ is the case where left handed lepton doublets do not interact with Z' and $x_H = 0$ is the B-L case. The deviation from the SM results could reach up to 4% for $x_H = 2$. Such deviations carry contributions from the Z' mediated process and its interference with the Z and photon mediated modes. The deviations from the SM falls sharply for $\cos \theta \geq 0.9$ and at the vicinity of 1.0, the effect from different charges are indistinguishable.

The total scattering cross section and the deviation of the total scattering cross section under the $U(1)_X$ case from

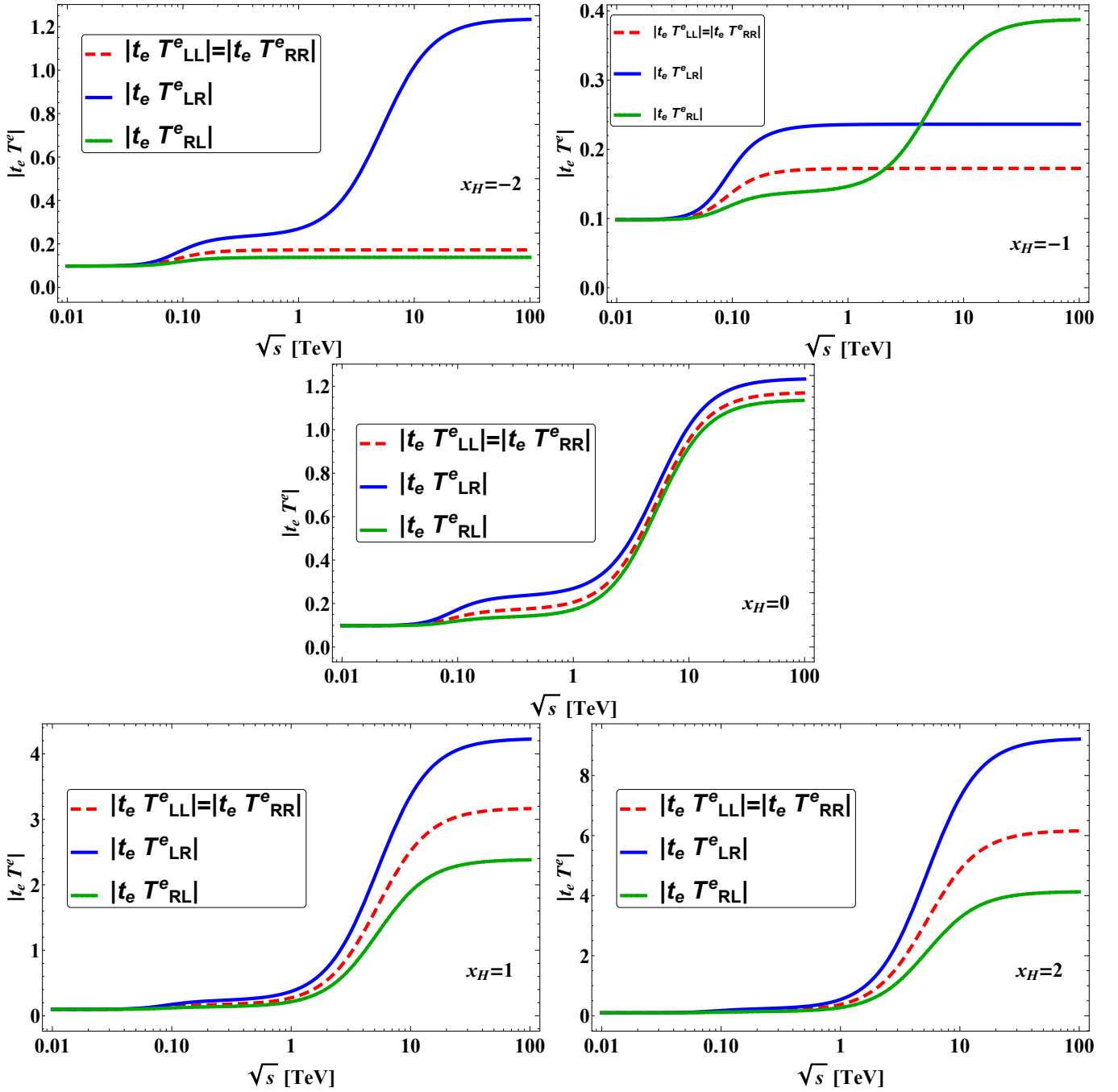


Figure 4. $|t_e T^e|$ as a function of \sqrt{s} for $\mu^+e^- \rightarrow \mu^+e^-$ process with $\cos\theta = 0.5$ for $M_{Z'} = 7.5$ TeV and different x_H .

the SM result for the $\mu^+e^- \rightarrow \mu^+e^-$ process are given by

$$\sigma^e(P_\mu, P_e) \equiv \int_{-0.99}^{0.99} \frac{d\sigma^e}{d\cos\theta}(P_\mu, P_e) d(\cos\theta), \quad (23)$$

$$\Delta_{\sigma^e} \equiv \frac{[\sigma^e(P_\mu, P_e)]_{U(1)_X}}{[\sigma^e(P_\mu, P_e)]_{SM}} - 1, \quad (24)$$

respectively. Since the cross section diverges at $\cos\theta \simeq 1$ therefore we integrate the differential scattering cross section within the range $-0.99 \leq \cos\theta \leq 0.99$ for different x_H and SM for different polarization of muon and electron as

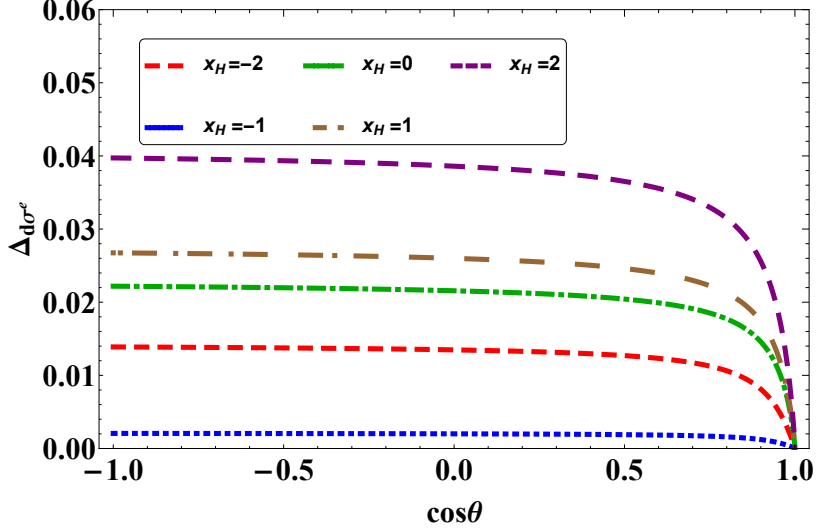


Figure 5. Deviation of total cross sections for $\mu^+e^- \rightarrow \mu^+e^-$ process from the SM as a function of $\cos\theta$ for $\sqrt{s} = 346$ GeV and $M_{Z'} = 7.5$ TeV with 1 ab^{-1} using different x_H .

$P_\mu = P_e = 0$, $P_\mu = 0.8, P_e = -0.8$ and $P_\mu = -0.8, P_e = 0.8$. The corresponding scattering cross sections for different x_H are shown in the upper panel of Fig. 6 with the corresponding deviations as a function of \sqrt{s} with $M_{Z'} = 7.5$ TeV for different polarization modes mentioned above from left to right. In Eq. (21), the dominant contribution comes from $\frac{d(\sigma_{\mu L e R})}{d(\cos\theta)}$ because $(1 - (-0.8))(1 + 0.8) = 3.24$ is larger than $(1 - (-0.8))(1 - 0.8) = (1 + (-0.8))(1 + 0.8) = 0.36$ and $(1 + (-0.8))(1 - 0.8) = 0.04$ respectively. In addition to that, T_{LR} for $x_H = 0$ and -2 are the same because $g_R V_\mu g_R^V = (\pm g_X)^2$ where plus sign corresponds to $x_H = -2$ and minus sign corresponds to $x_H = 0$. Therefore the cross sections are similar. The BSM case consists of the contribution from the Z' mediated process, in addition to Z and photon mediated processes including the contributions from corresponding interference terms. The SM result is shown by the black solid line which decreases with the increase in \sqrt{s} due to the absence of the contribution from Z' . The cross sections start deviations from the SM results and attains a maximum at $\sqrt{s} = M_{Z'} = 7.5$ TeV and slowly decreases when $\sqrt{s} > M_{Z'}$. The deviations of these cross sections stay within 5% for $\sqrt{s} = 346$ GeV and slowly grows with the increase in \sqrt{s} and finally maintains a constant value up to $\sqrt{s} = 100$ TeV. For $\sqrt{s} > M_{Z'}$ the deviation varies between 25% – 100% depending on x_H for different polarization of incoming muon and electron.

The $\mu^+e^- \rightarrow \mu^-e^+$ scattering mediated by Z' , Z and photon are forward dominant t -channel processes. Therefore we study the left-right asymmetry (\mathcal{A}_{LR}^e) of polarized cross sections and the differential left-right asymmetry is given by

$$\mathcal{A}_{LR}^e(P_\mu, P_e, \cos\theta) \equiv \frac{\frac{d\sigma^e}{d\cos\theta}(P_\mu, P_e) - \frac{d\sigma^e}{d\cos\theta}(-P_\mu, -P_e)}{\frac{d\sigma^e}{d\cos\theta}(P_\mu, P_e) + \frac{d\sigma^e}{d\cos\theta}(-P_\mu, -P_e)}, \quad (25)$$

and the deviation of the differential left-right asymmetry from the SM is given by

$$\Delta\mathcal{A}_{LR}^e \equiv \frac{[\mathcal{A}_{LR}^e]_{U(1)_X}}{[\mathcal{A}_{LR}^e]_{SM}} - 1. \quad (26)$$

The differential left-right asymmetry and its deviation with respect to $\cos\theta$ are shown in the lower left and middle panels of Fig. 6 respectively for different x_H with $P_\mu = 0.8, P_e = -0.8$. We find that differential left-right asymmetry varies between $-0.471 \leq \mathcal{A}_{LR} \leq -0.445$ for $-0.99 \leq \cos\theta \leq 0.99$ which sharply rises after $\cos\theta \geq 0.5$. We find that for $x_H = -2$ and -1 the differential left-right asymmetry may attain the values -0.471 and -0.464 respectively for $\cos\theta \leq 0.5$. That for the B-L case is -0.461 for $\cos\theta \leq 0.5$. In the case of $x_H = 1$ and 2 all the left and right handed fermions interact differently with Z' , however, they have different values. The SM contribution is shown by the solid black line which deviates from the BSM results when $\cos\theta \leq 0.35$. The deviation in differential left-right asymmetry ($\Delta\mathcal{A}_{LR}^e$) are shown in the top right panel for different x_H with respect to $\cos\theta$. The deviation in differential left-right scattering remains constant for $\cos\theta < 0.5$. The maximum deviation for $x_H = -2$ reaches up to 1.5% whereas that for $x_H = -1$ becomes 0.5%, $x_H = 0$ becomes 1%, $x_H = 2$ becomes 0.85% and $x_H = 1$ becomes 0.1% respectively.

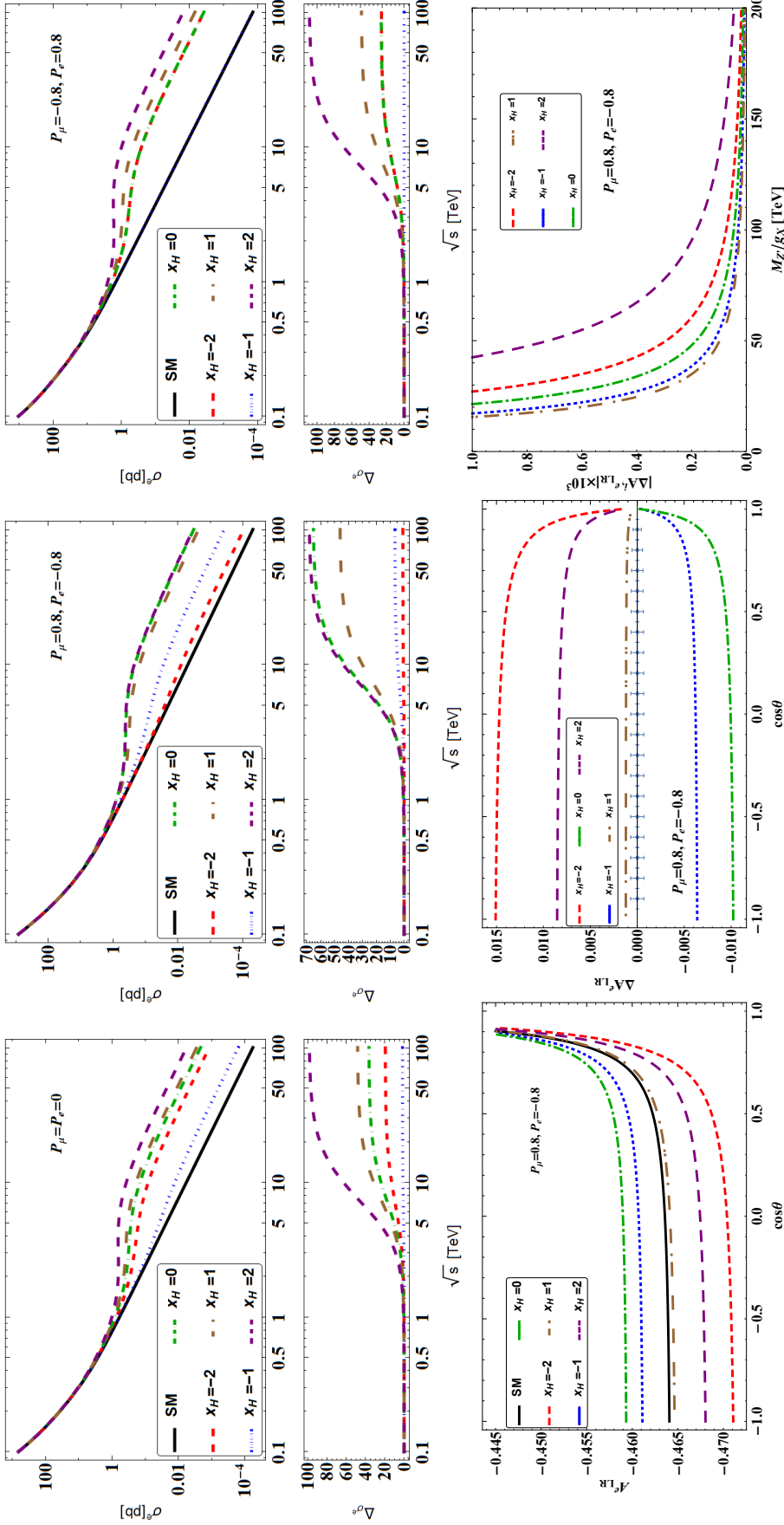


Figure 6. The total cross section for $\mu^+ e^- \rightarrow \mu^+ e^-$ process and the corresponding deviation from the SM for different polarization choices as a function of \sqrt{s} for $M_{Z'} = 7.5$ TeV and different x_H for $P_\mu = P_e = 0$, $P_\mu = 0.8$, $P_e = -0.8$ and $P_\mu = -0.8$, $P_e = 0.8$ from left to right respectively. In the lower panel we show the differential left-right asymmetry for $\mu^+ e^- \rightarrow \mu^+ e^-$ scattering process with respect to $\cos\theta$ in the lower left panel whereas its deviation with respect to $\cos\theta$ are given in the lower middle panel for different x_H . Deviation in integrated left-right asymmetry for this process as a function of $M_{Z'}/g_X$ for different values of x_H are shown in the lower right panel. To estimate the differential left-right asymmetry and the corresponding deviations we take $M_{Z'} = 7.5$ TeV. In this analysis we use $\sqrt{s} = 346$ GeV in appropriate places.

We show the error bar for the deviation in differential left-right asymmetry in the figure from Eq. A1 which is small compared to different values of the deviation in left-right asymmetry for different x_H .

The integrated left-right asymmetry for the $\mu^+e^- \rightarrow \mu^+e^-$ process is given by

$$\mathcal{A}_{LR}^{i,e} \equiv \frac{\int \frac{d\sigma^e}{d\cos\theta}(P_\mu, P_e)d(\cos\theta) - \int \frac{d\sigma^e}{d\cos\theta}(-P_\mu, -P_e)d(\cos\theta)}{\int \frac{d\sigma^e}{d\cos\theta}(P_\mu, P_e)d(\cos\theta) + \int \frac{d\sigma^e}{d\cos\theta}(-P_\mu, -P_e)d(\cos\theta)}, \quad (27)$$

and the deviation of the integrated left-right asymmetry from the SM is given by

$$\Delta\mathcal{A}_{LR}^{i,e} \equiv \frac{[\mathcal{A}_{LR}^{i,e}]_{U(1)_X}}{[\mathcal{A}_{LR}^{i,e}]_{SM}} - 1. \quad (28)$$

The deviation in integrated left-right asymmetry for different x_H with respect to $M_{Z'}/g_X$ are shown in the lower right panel of Fig. 6 with $P_\mu = 0.8$, $P_e = -0.8$. The $|\Delta\mathcal{A}_{LR}^{i,e}|$ falls sharply for $M_{Z'}/g_X > 50$ TeV for the values of x_H we consider and $M_{Z'}/g_X > 70$ TeV for $x_H = 2$, respectively. In this context from we quote the values of $M_{Z'}/g_X$ from LEP-II from Tab. II and these are $M_{Z'}/g_X \geq 5.0$ TeV, 2.2 TeV, 7 TeV, 11.1 TeV and 18.0 TeV for $x_H = -2, -1, 0, 1$ and 2, respectively. These bounds are not shown in the lower panel of Fig. 6 because LEP-II bounds are weaker and they do not cross the curves shown here. We do not add the prospective ILC bounds in the figure, however, they can be found from Tab. II.

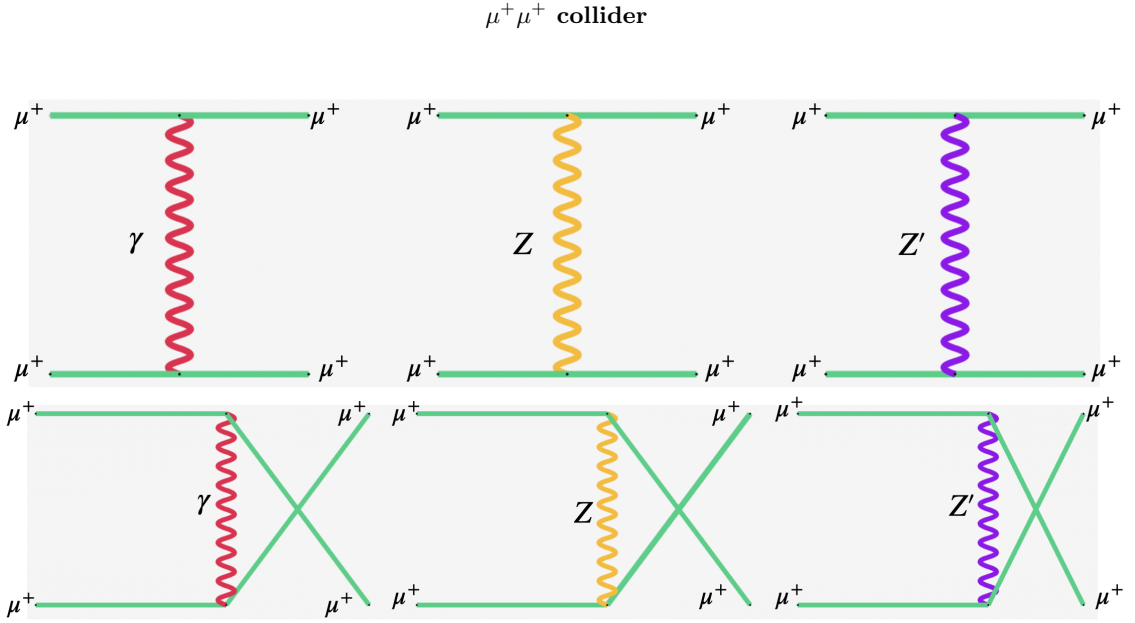


Figure 7. Photon, Z and Z' mediated $\mu^+\mu^+ \rightarrow \mu^+\mu^+$ processes in t -channel (upper panel) and u -channel (lower panel) at μ TRISTAN experiment with $\sqrt{s} = 2$ TeV.

We consider the $\mu^+\mu^+ \rightarrow \mu^+\mu^+$ scattering in the center-of-mass frame. Fig. 7 shows the $\mu^+\mu^+ \rightarrow \mu^+\mu^+$ scattering processes. We define the quantities p_1 and p_2 as initial momenta of the incoming muons, k_1 and k_2 are the final muon momenta. The 4-vector representation of these momenta are $p_1 = (E, 0, 0, E)$, $p_2 = (E, 0, 0, -E)$, $k_1 = (E, 0, E \sin\theta, E \cos\theta)$ and $k_2 = (E, 0, -E \sin\theta, -E \cos\theta)$, where E is the initial muon energy and θ is the scattering angle of the muon. There are photon, Z and Z' mediated t - and u -channel processes shown in Fig. 7. Contributions coming from the interference of these processes are also taken into consideration at the time of calculating the cross sections and respective observables. The Mandelstam variables are given by

$$s_\mu = 4E^2, \quad t_\mu = -\frac{s_\mu}{2}(1 - \cos\theta), \quad u_\mu = -\frac{s_\mu}{2}(1 + \cos\theta). \quad (29)$$

We fix the energies of incoming muons at $E = 1$ TeV each and the center-of-mass energy becomes $\sqrt{s_\mu} = 2$ TeV. We

define the following quantities

$$\begin{aligned}
T_{RR}^\mu &\equiv \sum_{V=\{\gamma,Z,Z'\}} \frac{(g_L^{V\mu})^2}{t_\mu - M_V^2}, & T_{LL}^\mu &\equiv \sum_{V=\{\gamma,Z,Z'\}} \frac{(g_R^{V\mu})^2}{t_\mu - M_V^2}, \\
T_{RL}^\mu &= T_{LR}^\mu &\equiv \sum_{V=\{\gamma,Z,Z'\}} \frac{g_R^{V\mu} g_L^{V\mu}}{t_\mu - M_V^2}, \\
U_{RR}^\mu &\equiv \sum_{V=\{\gamma,Z,Z'\}} \frac{(g_L^{V\mu})^2}{u_\mu - M_V^2}, & U_{LL}^\mu &\equiv \sum_{V=\{\gamma,Z,Z'\}} \frac{(g_R^{V\mu})^2}{u_\mu - M_V^2}, \\
U_{RL}^\mu &= U_{LR}^\mu &\equiv \sum_{V=\{\gamma,Z,Z'\}} \frac{g_R^{V\mu} g_L^{V\mu}}{u_\mu - M_V^2}.
\end{aligned} \tag{30}$$

We present the quantities $|t_\mu T^\mu|$ and $|u_\mu U^\mu|$ in Fig. 8. We find that the effect of the propagators from the t - and u -channel processes are same what we observed in $\mu^+ e^- \rightarrow \mu^+ e^-$ process where we also had t -channel mediated processes only. Depending on the $U(1)_X$ charges contributions from the respective propagators increases with increase in \sqrt{s} showing the effects of t - and u -channel processes.

Considering the initial muons are longitudinally polarized, the differential scattering cross sections with polarized initial states are given by

$$\frac{d\sigma_{\mu_R\mu_R}}{d\cos\theta} = \frac{s_\mu}{8\pi} |T_{RR}^\mu + U_{RR}^\mu|^2, \quad \frac{d\sigma_{\mu_L\mu_L}}{d\cos\theta} = \frac{s_\mu}{8\pi} |T_{LL}^\mu + U_{LL}^\mu|^2, \quad \frac{d\sigma_{\mu_R\mu_L}}{d\cos\theta} = \frac{d\sigma_{\mu_L\mu_R}}{d\cos\theta} = \frac{1}{8\pi s_\mu} \left(u_\mu^2 |T_{RL}^\mu|^2 + t_\mu^2 |U_{RL}^\mu|^2 \right). \tag{31}$$

Hence the differential scattering cross section for the $\mu^+ \mu^+ \rightarrow \mu^+ \mu^+$ process is given by

$$\frac{d\sigma^\mu}{d\cos\theta}(P_1, P_2) = \frac{1}{4} \left((1+P_1)(1+P_2) \frac{d\sigma_{\mu_R\mu_R}}{d\cos\theta} + (1-P_1)(1-P_2) \frac{d\sigma_{\mu_L\mu_L}}{d\cos\theta} + 2(1-P_1 P_2) \frac{d\sigma_{\mu_R\mu_L}}{d\cos\theta} \right), \tag{32}$$

where P_1 and P_2 are the corresponding polarizations of the muon beams under consideration. Here $P_i = +1$ denotes purely right-handed initial particles and $P_i = -1$ denotes purely left-handed initial particles, respectively. Hence we calculate the deviation in differential scattering cross section due the BSM effect from the SM contribution as

$$\Delta_{d\sigma^\mu} \equiv \frac{[\frac{d\sigma^\mu}{d\cos\theta}(0,0)]_{U(1)_X}}{[\frac{d\sigma^\mu}{d\cos\theta}(0,0)]_{SM}} - 1. \tag{33}$$

Fig. 9 shows the deviation of the BSM differential scattering cross section due to the effect of Z' under the $U(1)_X$ scenario from the SM. We notice that the deviations for $x_H = -2$ and -1 are below 3.6% and 0.5% depending on $\cos\theta$, respectively showing in the left panel where $x_H = -2$ shows the case where left handed lepton doublet has no interaction with Z' whereas for $x_H = -1$, right handed lepton has no interaction with Z' . The maximum deviation reaches up to 75% near $\cos\theta \simeq 0$ which increases with x_H from zero to 2. All the charges show the effect of t - and u -channel processes involving the interference effects.

The total scattering cross section and the deviation of the total scattering cross section due to the effect of Z' from the SM scenario are given by

$$\sigma^\mu(P_1, P_2) \equiv \int_0^{0.99} \frac{d\sigma^\mu}{d\cos\theta}(P_1, P_2) d(\cos\theta), \tag{34}$$

$$\Delta_{\sigma^\mu} \equiv \frac{[\sigma^\mu(P_1, P_2)]_{U(1)_X}}{[\sigma^\mu(P_1, P_2)]_{SM}} - 1, \tag{35}$$

respectively. The corresponding integrated scattering cross sections are shown in the upper panel of Fig. 10 for different polarizations $-0.8, 0$ and 0.8 from left to right along with the SM contribution for $-0.99 \leq \cos\theta \leq 0.99$. The integrated cross sections start deviating from the SM result from $\sqrt{s} > 1$ TeV depending on x_H . The integrated scattering cross section decreases with \sqrt{s} showing the nature of t - and u -channel processes, however, due to the influence of $U(1)_X$ charges and Z' , the rates of decrease in integrated scattering cross sections are different for different polarizations depending on x_H . Integrated scattering cross sections for the SM process is shown by the black solid

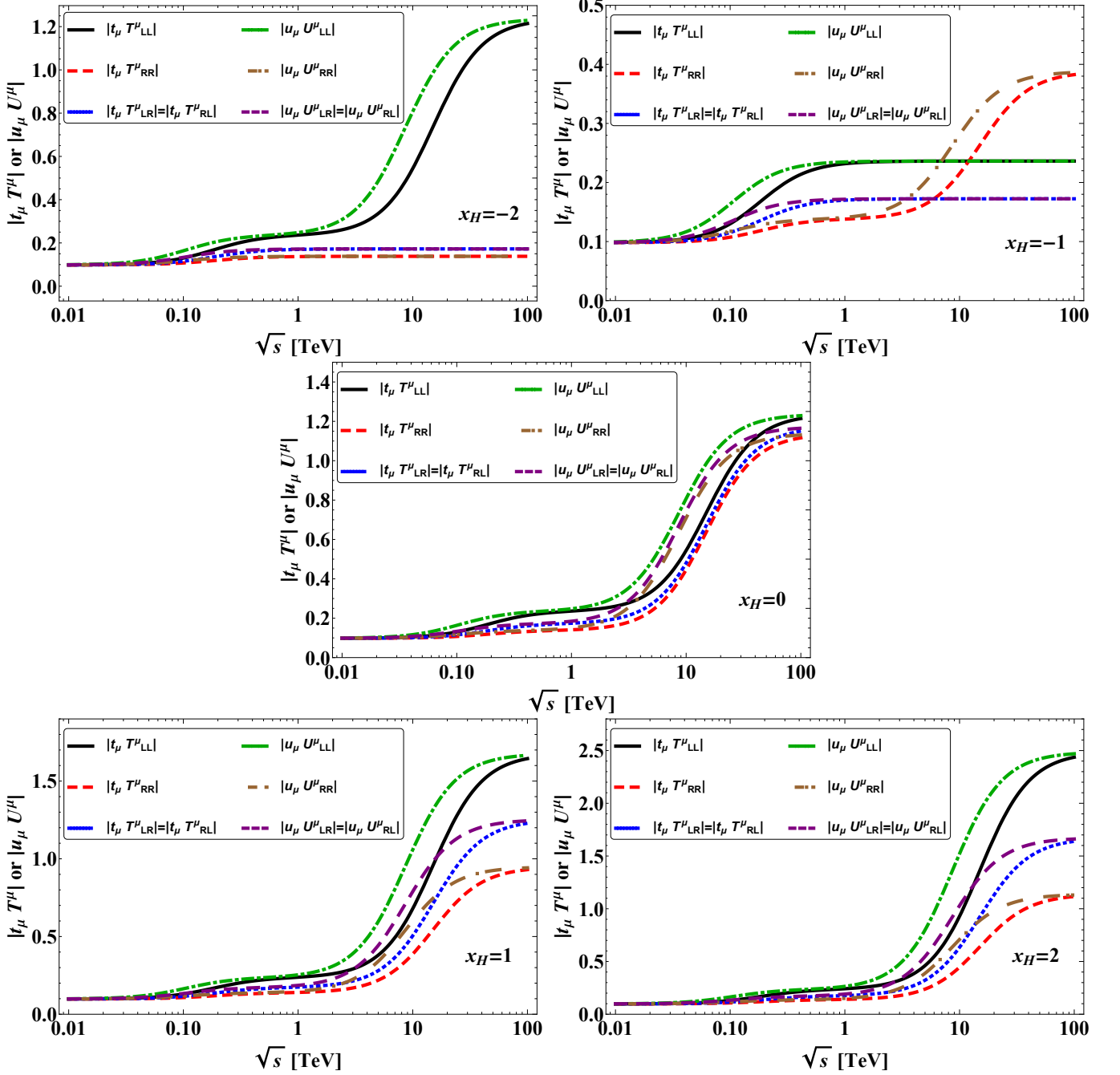


Figure 8. $|t_\mu T^\mu|$ and $|u_\mu U^\mu|$ as a function of \sqrt{s} for $\mu^+\mu^+ \rightarrow \mu^+\mu^+$ scattering process with $\cos\theta = 0.5$ and $M_{Z'} = 7.5$ TeV and different x_H .

line. As a result the deviations in integrated scattering cross sections from the SM with respect to x_H with the increases in \sqrt{s} .

The differential left-right asymmetry of polarized cross sections is given by

$$A_{LR}^\mu(P_1, P_2, \cos\theta) \equiv \frac{\frac{d\sigma}{d\cos\theta}(P_1, P_2) - \frac{d\sigma}{d\cos\theta}(-P_1, -P_2)}{\frac{d\sigma}{d\cos\theta}(P_1, P_2) + \frac{d\sigma}{d\cos\theta}(-P_1, -P_2)}, \quad (36)$$

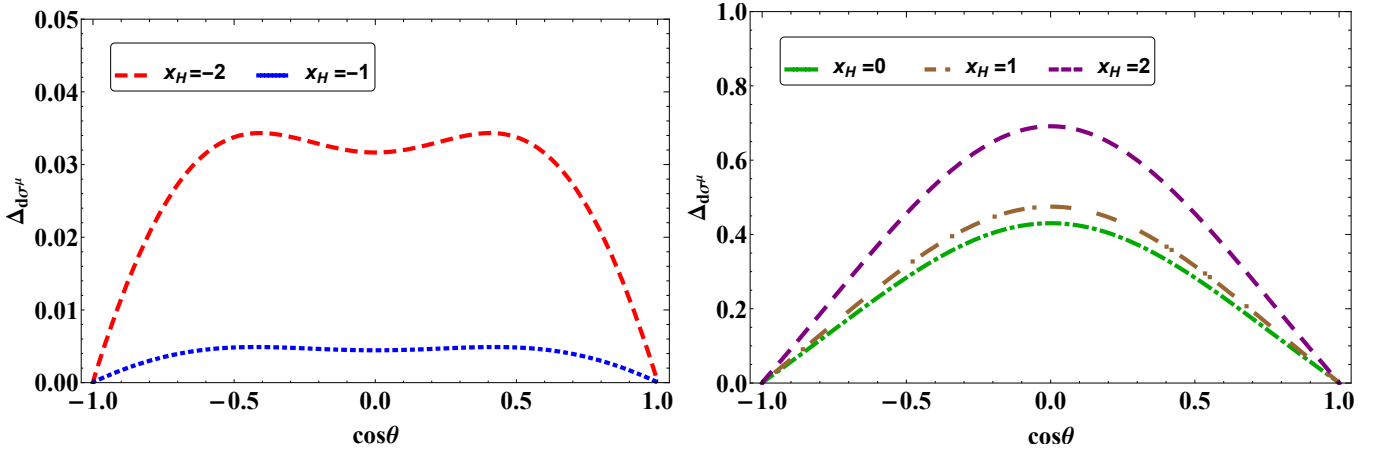


Figure 9. Deviation of total scattering cross sections for $\mu^+\mu^+ \rightarrow \mu^+\mu^+$ process due to the Z' induced processes from the SM results as a function of $\cos\theta$ at 100 fb^{-1} luminosity for different x_H .

and the deviation of the differential left-right asymmetry from the SM is given by

$$\Delta A_{\text{LR}}^\mu \equiv \frac{[A_{\text{LR}}^\mu]_{U(1)_X}}{[A_{\text{LR}}^\mu]_{\text{SM}}} - 1. \quad (37)$$

The corresponding signatures are given in the lower left and middle panels of Fig. 10 for different x_H in the context of $U(1)_X$ scenario with $P_1 = P_2 = 0.8$ for $M_{Z'} = 7.5 \text{ TeV}$. The differential left right asymmetry reaches a maximum around -0.2 the vicinity of $\cos\theta = 0$ for different values of x_H whereas that for $x_H = -2$ is around -3.5 . Due to the deviation from zero, the differential left-right asymmetry falls on both sides of $\cos\theta = 0$ and showing sharp peaks for $\cos\theta = \pm 1$ suggesting to consider $-1 \leq \cos\theta \leq 1$ while calculating integrated left-right asymmetry. We estimate the deviation in differential left-right asymmetry from the SM can reach up to 35% at the vicinity of $\cos\theta = 0$ for $x_H = -2$ where left handed lepton doublet do not interact with Z' . The deviation in differential left-right asymmetry in the BSM case from the SM scenario for $x_H = -2$ slowly falls off to zero when $\cos\theta \rightarrow \pm 1$. Similar behavior can be observed for $x_H = 2$ but the maximum deviation may reach up to 5%. We notice that ΔA_{LR} is negative for $x_H = -1$ and $x_H = 0$, however, considering $|\Delta A_{\text{LR}}|$ the percentage of corresponding deviations can be estimated. For example, the maximum deviations for $x_H = -1$ and 0 can reach up to 5% and 60% at the vicinity of $\cos\theta = 0$ which will approach zero with the limits $\cos\theta \rightarrow \pm 1$. A mixed behavior will be observed for $x_H = 1$ where the deviation in left-right asymmetry from the SM can be zero at the vicinity of $\cos\theta = 0$ and maximum can reach up to $|\Delta A_{\text{LR}}| = 4\%$ around $\cos\theta = \pm 0.5$. In addition to that, the deviation will approach zero for $\cos\theta \rightarrow \pm 1$. Apart from the dependence on x_H , this type of behavior occurs due to the combined effect of t - and u -channel processes including the effects from their interference. The errors in the deviation in left-right asymmetry have been estimated using Eq. A1.

Finally, the integrated left-right asymmetry is given by

$$A_{\text{LR}}^{i,\mu} \equiv \frac{\int \frac{d\sigma^\mu}{d\cos\theta}(P_1, P_2)d(\cos\theta) - \int \frac{d\sigma^\mu}{d\cos\theta}(-P_1, -P_2)d(\cos\theta)}{\int \frac{d\sigma^\mu}{d\cos\theta}(P_1, P_2)d(\cos\theta) + \int \frac{d\sigma^\mu}{d\cos\theta}(-P_1, -P_2)d(\cos\theta)}, \quad (38)$$

and the deviation of the integrated left-right asymmetry from the SM is given by

$$\Delta A_{\text{LR}}^{i,\mu} \equiv \frac{[A_{\text{LR}}^{i,\mu}]_{U(1)_X}}{[A_{\text{LR}}^{i,\mu}]_{\text{SM}}} - 1 \quad (39)$$

to estimate the deviations in integrated left-right asymmetry as a function of $M_{Z'}/g_X$ for different x_H and these are shown in the lower right panel of Fig. 10 for $P_1 = P_2 = 0.8$ ¹. The $|\Delta A_{\text{LR}}^{i,\mu}|$ falls sharply for approximately $M_{Z'}/g_X > 50$

¹ The one-loop cross sections from the SM processes have been estimated in [50] for $\mu^+\mu^+$ and e^-e^- colliders. The relative correction between the Born process and next-to-leading order electroweak (NLO-EW) process is about $\mathcal{O}(10\%)$. Involving the NLO-EW cross section in $\mu^+\mu^+$ collider with $\sqrt{s} = 2 \text{ TeV}$, we find $A_{\text{LRSM}}^{i,\mu \text{ NLO-EW}} = -0.0003$ whereas $A_{\text{LRSM}}^{i,\mu \text{ Born}} = -0.11$. The NLO-EW integrated left-right asymmetry becomes very small due to a cancellation between SM Born and one-loop contributions. Hence $\Delta A_{\text{LR}}^{i,\mu}$ could be enhanced.

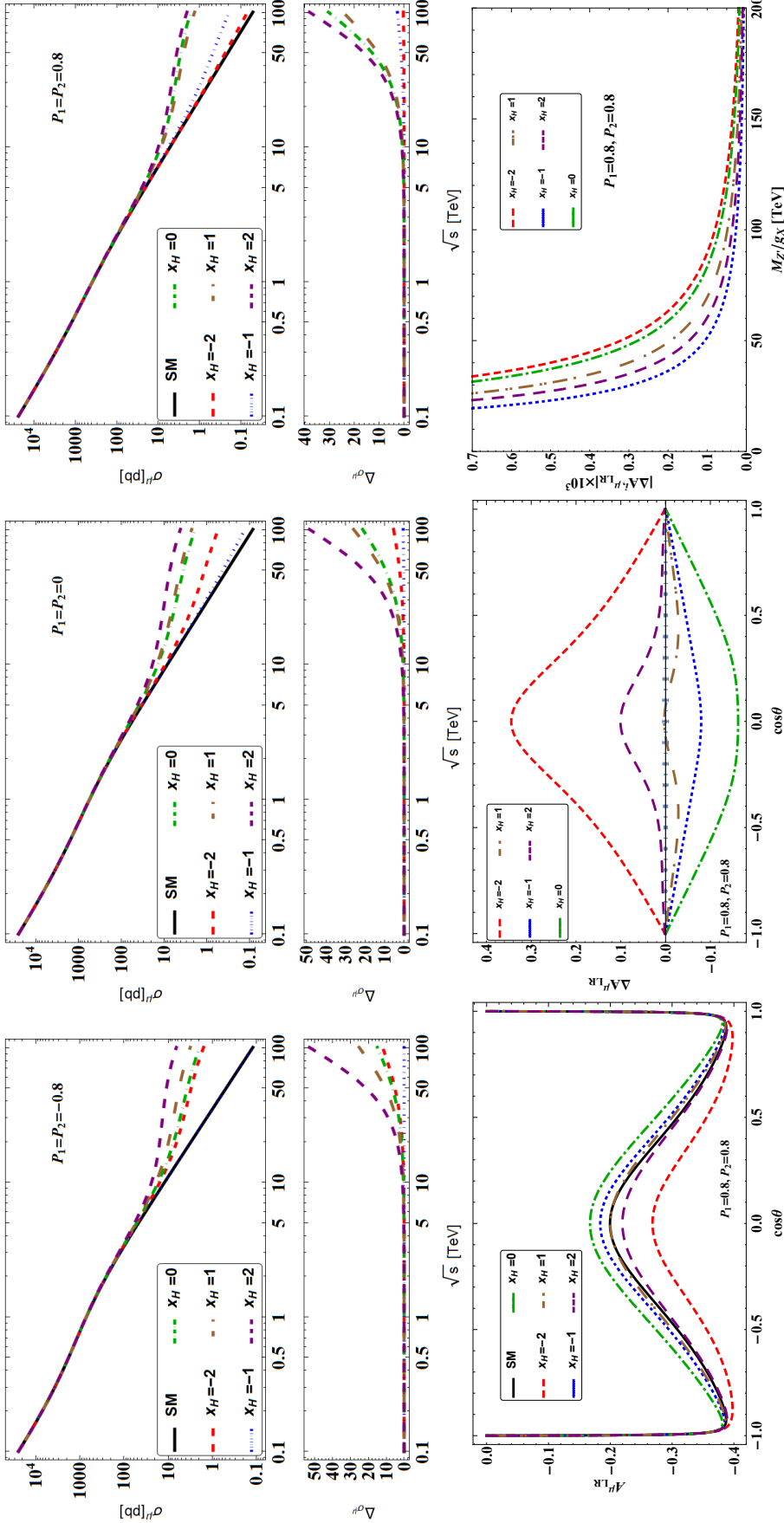


Figure 10. The total cross section for $\mu^+ \mu^+ \rightarrow \mu^+ \mu^+$ process and the corresponding deviation are shown in the upper panel from the SM for different polarization choices as a function of \sqrt{s} for $M_{Z'} = 7.5$ TeV and different x_H for $P_1 = P_2 = 0$, $P_1 = P_2 = 0.8$ and $P_1 = P_2 = -0.8$ from left to right respectively. In the lower panel we show the differential left-right asymmetry for $\mu^+ \mu^+ \rightarrow \mu^+ \mu^+$ scattering process with respect to $\cos \theta$ in the lower left panel whereas its deviation with respect to $\cos \theta$ are given in the lower middle panel for different x_H . Deviation in integrated left-right asymmetry for this process as a function of $M_{Z'}/g_X$ for different values of x_H are shown in the lower right panel. To estimate the differential left-right asymmetry and the corresponding deviations we take $M_{Z'} = 7.5$ TeV. In this analysis we use $\sqrt{s} = 1$ TeV in appropriate places.

TeV with respect to different x_H under consideration. The bounds on $M_{Z'}/g_X$ from LEP-II could be found from Tab. II for different x_H which are well below 50 TeV. Therefore μ TRISTAN collider could probe a higher $U(1)_X$ breaking scale.

IV. CONCLUSIONS

We study a general $U(1)$ extension of the SM to investigate the BSM effect coming from the Z' gauge boson in the forward dominant collisions in μ^+e^- and $\mu^+\mu^+$ collisions. We find that the propagators from t - and u -channel processes involve the effect of Z' gauge boson manifesting different behaviors for different helicity combinations depending on general $U(1)$ charges of the leptons. The deviations in differential and integrated scattering cross sections from the SM suggest that the influence of Z' could be sizable in these colliders through the t - and u -channel processes depending on the nature of the colliders. As a result, the left-right asymmetry will be an interesting observable to test the effect of BSM physics from the Z' contribution. In our model due to the general $U(1)$ scenario, left and right handed fermions interact differently with Z' manifesting chiral scenario. Therefore we obtain sizable left-right asymmetry in the context of μ^+e^- and $\mu^+\mu^+$ scattering. The differential left-right asymmetry and the deviation in differential left-right asymmetry from the SM are different due to the effect of general $U(1)_X$ charges which could provide information about the interactions between Z' and charged leptons which could be probed in μ TRISTAN experiment. The limits on the deviation in the integrated left-right asymmetry from the SM from the μ^+e^- and $\mu^+\mu^+$ collision can improve the bound on the general $U(1)$ breaking scale. The deviations in these analyses are more than the theoretically estimated error bars denoting that such a chiral scenario could have fascinating aspects in the forward dominant scattering. Following the sizable deviations from the SM results we could probe the nature of the interactions between Z' and charged leptons and also know about the breaking scale of $U(1)_X$ scenario from the μ TRISTAN experiment in future.

Appendix A: Error analyses

The error bar of Left-Right asymmetry at $\theta = \theta_0$ is given by

$$\delta\Delta A_{LR}^i(\cos\theta_0) = 2 \frac{\sqrt{N_{LR}^i(\cos\theta_0)N_{RL}^i(\cos\theta_0)} \left(\sqrt{N_{LR}^i(\cos\theta_0)} + \sqrt{N_{RL}^i(\cos\theta_0)} \right)}{(N_{LR}^i(\cos\theta_0) + N_{RL}^i(\cos\theta_0))^2}, \quad (\text{A1})$$

where i is e or μ ,

$$N_{LR}^i(\cos\theta_0) \equiv \mathcal{L}_{int} \int_{\cos\theta_0-0.05}^{\cos\theta_0+0.05} \frac{d\sigma^i}{d\cos\theta}(P_1, P_2, \cos\theta) d\cos\theta, \quad (\text{A2})$$

$$N_{RL}^i(\cos\theta_0) \equiv \mathcal{L}_{int} \int_{\cos\theta_0-0.05}^{\cos\theta_0+0.05} \frac{d\sigma^i}{d\cos\theta}(-P_1, -P_2, \cos\theta) d\cos\theta, \quad (\text{A3})$$

and \mathcal{L}_{int} is the integrated luminosity.

-
- [1] **Particle Data Group** Collaboration, P. Zyla *et al.*, “Review of Particle Physics,” *PTEP* **2020** no. 8, (2020) 083C01.
[2] A. Leike, “The Phenomenology of extra neutral gauge bosons,” *Phys. Rept.* **317** (1999) 143–250, [arXiv:hep-ph/9805494](#) [[hep-ph](#)].
[3] P. Langacker, “The Physics of Heavy Z' Gauge Bosons,” *Rev. Mod. Phys.* **81** (2009) 1199–1228, [arXiv:0801.1345](#) [[hep-ph](#)].
[4] J. C. Pati and A. Salam, “Lepton Number as the Fourth Color,” *Phys. Rev. D* **10** (1974) 275–289. [Erratum: *Phys.Rev.D* **11**, 703–703 (1975)].
[5] R. Mohapatra and J. C. Pati, “A Natural Left-Right Symmetry,” *Phys. Rev. D* **11** (1975) 2558.
[6] G. Senjanovic and R. N. Mohapatra, “Exact Left-Right Symmetry and Spontaneous Violation of Parity,” *Phys. Rev. D* **12** (1975) 1502.
[7] H. Georgi, “The State of the Art—Gauge Theories,” *AIP Conf. Proc.* **23** (1975) 575–582.
[8] H. Fritzsch and P. Minkowski, “Unified Interactions of Leptons and Hadrons,” *Annals Phys.* **93** (1975) 193–266.
[9] F. Gursey, P. Ramond, and P. Sikivie, “A Universal Gauge Theory Model Based on E_6 ,” *Phys. Lett. B* **60** (1976) 177–180.

- [10] Y. Achiman and B. Stech, “Quark Lepton Symmetry and Mass Scales in an E6 Unified Gauge Model,” *Phys. Lett. B* **77** (1978) 389–393.
- [11] A. Davidson, “ $B - L$ as the fourth color within an $SU(2)_L \times U(1)_R \times U(1)$ model,” *Phys. Rev. D* **20** (1979) 776.
- [12] A. Davidson, M. Koca, and K. C. Wali, “ $U(1)$ as the Minimal Horizontal Gauge Symmetry,” *Phys. Rev. Lett.* **43** (1979) 92.
- [13] R. Marshak and R. N. Mohapatra, “Quark - Lepton Symmetry and $B - L$ as the $U(1)$ Generator of the Electroweak Symmetry Group,” *Phys. Lett. B* **91** (1980) 222–224.
- [14] R. N. Mohapatra and R. Marshak, “Local $B - L$ Symmetry of Electroweak Interactions, Majorana Neutrinos and Neutron Oscillations,” *Phys. Rev. Lett.* **44** (1980) 1316–1319. [Erratum: *Phys.Rev.Lett.* 44, 1643 (1980)].
- [15] **ALEPH, DELPHI, L3, OPAL, LEP Electroweak** Collaboration, S. Schael *et al.*, “Electroweak Measurements in Electron-Positron Collisions at W-Boson-Pair Energies at LEP,” *Phys. Rept.* **532** (2013) 119–244, [arXiv:1302.3415 \[hep-ex\]](#).
- [16] **DO** Collaboration, V. M. Abazov *et al.*, “Search for a Heavy Neutral Gauge Boson in the Dielectron Channel with 5.4 fb^{-1} of $p\bar{p}$ Collisions at $\sqrt{s} = 1.96$ TeV,” *Phys. Lett. B* **695** (2011) 88–94, [arXiv:1008.2023 \[hep-ex\]](#).
- [17] **CDF** Collaboration, T. Aaltonen *et al.*, “Search for High Mass Resonances Decaying to Muon Pairs in $\sqrt{s} = 1.96$ TeV $p\bar{p}$ Collisions,” *Phys. Rev. Lett.* **106** (2011) 121801, [arXiv:1101.4578 \[hep-ex\]](#).
- [18] **ATLAS** Collaboration, G. Aad *et al.*, “Search for high-mass dilepton resonances using 139 fb^{-1} of pp collision data collected at $\sqrt{s} = 13$ TeV with the ATLAS detector,” *Phys. Lett. B* **796** (2019) 68–87, [arXiv:1903.06248 \[hep-ex\]](#).
- [19] **CMS** Collaboration, C. Collaboration, “Search for a narrow resonance in high-mass dilepton final states in proton-proton collisions using 140 fb^{-1} of data at $\sqrt{s} = 13$ TeV,” CMS-PAS-EXO-19-019.
- [20] Y. Li, F. Petriello, and S. Quackenbush, “Reconstructing a Z-prime Lagrangian using the LHC and low-energy data,” *Phys. Rev. D* **80** (2009) 055018, [arXiv:0906.4132 \[hep-ph\]](#).
- [21] T. Appelquist, B. A. Dobrescu, and A. R. Hopper, “Nonexotic Neutral Gauge Bosons,” *Phys. Rev. D* **68** (2003) 035012, [arXiv:hep-ph/0212073](#).
- [22] C. Coriano, L. Delle Rose, and C. Marzo, “Vacuum Stability in $U(1)$ -Prime Extensions of the Standard Model with TeV Scale Right Handed Neutrinos,” *Phys. Lett. B* **738** (2014) 13–19, [arXiv:1407.8539 \[hep-ph\]](#).
- [23] A. Das, S. Oda, N. Okada, and D.-s. Takahashi, “Classically conformal $U(1)$ ’ extended standard model, electroweak vacuum stability, and LHC Run-2 bounds,” *Phys. Rev. D* **93** no. 11, (2016) 115038, [arXiv:1605.01157 \[hep-ph\]](#).
- [24] A. Das, P. S. B. Dev, Y. Hosotani, and S. Mandal, “Probing the minimal $U(1)X$ model at future electron-positron colliders via fermion pair-production channels,” *Phys. Rev. D* **105** no. 11, (2022) 115030, [arXiv:2104.10902 \[hep-ph\]](#).
- [25] S. K. A., A. Das, G. Lambiase, T. Nomura, and Y. Orikasa, “Probing chiral and flavored Z' from cosmic bursts through neutrino interactions,” [arXiv:2308.14483 \[hep-ph\]](#).
- [26] C. A. Heusch and F. Cuyper, “Physics with like-sign muon beams in a TeV muon collider,” *AIP Conf. Proc.* **352** (1996) 219–231, [arXiv:hep-ph/9508230](#).
- [27] A. B. Arbuzov, S. G. Bondarenko, L. V. Kalinovskaya, L. A. Rummyantsev, and V. L. Yermolchik, “Electroweak effects in polarized muon-electron scattering,” *Phys. Rev. D* **105** no. 3, (2022) 033009, [arXiv:2112.09361 \[hep-ph\]](#).
- [28] S. G. Bondarenko, L. V. Kalinovskaya, L. A. Rummyantsev, R. Sadykov, and V. L. Yermolchik, “One-Loop Electroweak Radiative Corrections to Polarized Møller Scattering,” *JETP Lett.* **115** no. 9, (2022) 495–501, [arXiv:2111.11490 \[hep-ph\]](#).
- [29] Y. Hamada, R. Kitano, R. Matsudo, and H. Takaura, “Precision $\mu+\mu+$ and $\mu+e-$ elastic scatterings,” *PTEP* **2023** no. 1, (2023) 013B07, [arXiv:2210.11083 \[hep-ph\]](#).
- [30] Y. Hamada, R. Kitano, R. Matsudo, H. Takaura, and M. Yoshida, “ μ TRISTAN,” *PTEP* **2022** no. 5, (2022) 053B02, [arXiv:2201.06664 \[hep-ph\]](#).
- [31] K. Fridell, R. Kitano, and R. Takai, “Lepton flavor physics at $\mu^+\mu^+$ colliders,” *JHEP* **06** (2023) 086, [arXiv:2304.14020 \[hep-ph\]](#).
- [32] G. Lichtenstein, M. A. Schmidt, G. Valencia, and R. R. Volkas, “Complementarity of μ TRISTAN and Belle II in searches for charged-lepton flavour violation,” *Phys. Lett. B* **845** (2023) 138144, [arXiv:2307.11369 \[hep-ph\]](#).
- [33] P. S. B. Dev, J. Heeck, and A. Thapa, “Neutrino mass models at μ TRISTAN,” [arXiv:2309.06463 \[hep-ph\]](#).
- [34] E. Celada, T. Han, W. Kilian, N. Kreher, Y. Ma, F. Maltoni, D. Pagani, J. Reuter, T. Striegl, and K. Xie, “Probing Higgs-muon interactions at a multi-TeV muon collider,” [arXiv:2312.13082 \[hep-ph\]](#).
- [35] A. Goudelis, J. Kriewald, E. Pinsard, and A. M. Teixeira, “cLFV leptophilic Z' as a dark matter portal: prospects for colliders,” [arXiv:2312.14103 \[hep-ph\]](#).
- [36] M. Abe *et al.*, “A New Approach for Measuring the Muon Anomalous Magnetic Moment and Electric Dipole Moment,” *PTEP* **2019** no. 5, (2019) 053C02, [arXiv:1901.03047 \[physics.ins-det\]](#).
- [37] F. Bossi and P. Ciafaloni, “Lepton Flavor Violation at muon-electron colliders,” *JHEP* **10** (2020) 033, [arXiv:2003.03997 \[hep-ph\]](#).
- [38] M. Lu, A. M. Levin, C. Li, A. Agapitos, Q. Li, F. Meng, S. Qian, J. Xiao, and T. Yang, “The physics case for an electron-muon collider,” *Adv. High Energy Phys.* **2021** (2021) 6693618, [arXiv:2010.15144 \[hep-ph\]](#).
- [39] K. Cheung and Z. S. Wang, “Physics potential of a muon-proton collider,” *Phys. Rev. D* **103** (2021) 116009, [arXiv:2101.10476 \[hep-ph\]](#).
- [40] J.-C. Yang, Z.-B. Qing, X.-Y. Han, Y.-C. Guo, and T. Li, “Tri-photon at muon collider: a new process to probe the anomalous quartic gauge couplings,” *JHEP* **22** (2020) 053, [arXiv:2204.08195 \[hep-ph\]](#).
- [41] W. Liu and K.-P. Xie, “Probing electroweak phase transition with multi-TeV muon colliders and gravitational waves,” *JHEP* **04** (2021) 015, [arXiv:2101.10469 \[hep-ph\]](#).

- [42] J.-L. Yang, C.-H. Chang, and T.-F. Feng, “The leptonic di-flavor and di-number violation processes at high energy $\mu^\pm\mu^\pm$ colliders,” [arXiv:2302.13247 \[hep-ph\]](#).
- [43] A. Das, T. Nomura, and T. Shimomura, “Multi muon/anti-muon signals via productions of gauge and scalar bosons in a $U(1)_{L_\mu-L_\tau}$ model at muonic colliders,” *Eur. Phys. J. C* **83** no. 9, (2023) 786, [arXiv:2212.11674 \[hep-ph\]](#).
- [44] G. Lichtenstein, M. A. Schmidt, G. Valencia, and R. R. Volkas, “Constraints on doubly-charged-scalar lepton-triality models from 1-loop processes,” [arXiv:2312.09409 \[hep-ph\]](#).
- [45] E. Eichten, K. D. Lane, and M. E. Peskin, “New Tests for Quark and Lepton Substructure,” *Phys. Rev. Lett.* **50** (1983) 811–814.
- [46] **LEP, ALEPH, DELPHI, L3, OPAL, LEP Electroweak Working Group, SLD Electroweak Group, SLD Heavy Flavor Group** Collaboration, “A Combination of preliminary electroweak measurements and constraints on the standard model,” [arXiv:hep-ex/0312023](#).
- [47] H. Kroha, “Compositeness limits from E^+E^- annihilation revisited,” *Phys. Rev. D* **46** (1992) 58–69.
- [48] M. Carena, A. Daleo, B. A. Dobrescu, and T. M. Tait, “ Z' gauge bosons at the Tevatron,” *Phys. Rev. D* **70** (2004) 093009, [arXiv:hep-ph/0408098](#).
- [49] **LCC Physics Working Group** Collaboration, K. Fujii *et al.*, “Tests of the Standard Model at the International Linear Collider,” [arXiv:1908.11299 \[hep-ex\]](#).
- [50] S. G. Bondarenko, L. V. Kalinovskaya, L. A. Rumyantsev, and V. L. Yermolchik, “One-loop electroweak radiative corrections to polarized Møller scattering,” *JETP Lett.* **115** no. 9, (2022) 495–501, [arXiv:2203.10538 \[hep-ph\]](#).